Judd–Ofelt and photoluminescence analysis of Nd_2O_3-doped within host fluoroborate glass from the system B_2O_3–NaF–La_2O_3

M. A. Marzouk[1] · F. H. ElBatal[1] · Y. M. Hamdy[2] · H. A. ElBatal[1]

Abstract

Undoped glass of chemical composition $70B_2O_3$–25NaF–$5La_2O_3$ together with Nd_2O_3-doped samples were prepared via conventional melt and annealing procedure. The prepared glasses were investigated through photoluminescence measurements to find out their extent for the lasing application. The undoped sample reveals two UV absorption peaks while Nd_2O_3-doped samples show 10 well-characterized peaks in the UV–Visible range that are correlated to different transition states of Nd^{3+} ions. Three different bands are detected in the emission spectra at 875 nm ($^4F_{3/2} \rightarrow {}^4I_{9/2}$), 1056 nm ($^4F_{3/2} \rightarrow {}^4I_{11/2}$), and 1326 nm ($^4F_{3/2} \rightarrow {}^4I_{13/2}$). The Judd–Ofelt parameters ($\Omega 2$, $\Omega 4$, $\Omega 6$) and radiative properties were estimated using the Judd–Ofelt theory. The represented data indicated that the transition line $^4F_{3/2} \rightarrow {}^4I_{11/2}$ is the sharpest and lowest bandwidth value than other detected transitions. The structural analysis by FTIR vibrational modes suggested that the IR absorption bands within the range 800–1200 cm^{-1} originate from both combined vibrations of tetrahedral (BO_4) and (BO_3F) groups together with (NaF_4) groups beside triangular BO_3 groups which are vibrating within the range 1200–1600 cm^{-1}. The addition of Nd_2O_3 is assumed to cause the possible transformation of some structural B–O bonds within the range of triangular borate units referring to the possible formation of pyroborate units or similar structural groups.

Keywords Glass · Fluoroborate · Nd_2O_3 · Photoluminescence · Judd–Ofelt · FTIR

1 Introduction

Borate glasses belong to the three most interesting, highly distinguished and widely studied inorganic vitreous materials beside silicate and phosphate glasses [1–3]. However, borate glasses possess unique and exceptional structural configurations in which two variant building groups (BO_3 and BO_4) can be both identified in various borates with different ratios depending on the nature and percent of partner oxides [1–3]. The maximum limiting compositions of binary oxides with B_2O_3 are quite different and variable. The alkali oxides with B_2O_3 can form stable glasses by normal melting-annealing techniques approaching 30% while the alkaline earth oxides and other divalent with percent oxides such as ZnO and CdO can show higher percent for these oxides with B_2O_3 [4, 5]. Also, the binary alkali fluorides can form stable glasses with B_2O_3 with higher percentages than the related alkali oxides [6, 7]. Glasses containing rare earth (RE) ions have attracted great investigations due to their valuable lasing action in the visible and near-infrared regions [8–18]. Among all rare earth lanthanum oxide (La_2O_3) is a potential candidate for modifying various physical and optical properties of glasses and glass–ceramics and improving their chemical stability [9–12]. The incorporation of rare-earth neodymium oxide (Nd_2O_3) into glasses produces interesting colored samples which can show distinct dichroism in certain concentrated Nd_2O_3-glasses [13–16]. The suitability of Nd^{3+} ions in emitting strong near-infrared emission at 1.06 μm makes it the best possible candidate for high-power laser applications [8, 16, 17]. Among different rare-earth ions, Nd^{3+} ion is one of the most studied and also one of the most efficient ions for photonic devices [12–18].

It has been recognized by many glass scientists [2, 5, 7, 17, 18] that the introduction of fluoride ions into phosphate or borate glasses produces mixed candidates of

✉ M. A. Marzouk
marzouk_nrc@yahoo.com

1 Glass Research Department, National Research Centre, 33 EL Bohouth St. (Former EL Tahrir St.), Dokki, P.O. 12622, Giza, Egypt

2 Spectroscopy Department, National Research Centre, 33 El Bohouth Street (Former EL Tahrir), Dokki, P.O. 12622, Giza, Egypt

fluorophosphate or fluoroborate glasses with superior combining the better properties of mixed partners. Also, research on fluoroborate glasses by several authors [2, 5, 7, 17, 18] has reached the conclusion that primarily the limiting compositions for glass formation are much higher in binary borates like (LiF–B_2O_3), (NaF–B_2O_3) and (CaF$_2$–B_2O_3) and beside their properties are different and refer to their ability to share in optical component candidates. This work is a second step of studying rare earth (Nd^{3+} ions) in fluoroborate glass (LiF–CaF$_2$–B_2O_3) with the intention of justifying their difference from ordinary alkali or alkaline earth oxide borate glasses. In a previous publication by the sharing of the authors [19] we studied the behavior of Bi^{3+} ion in the two glassy systems (LiF–P_2O_5) and (LiF–B_2O_3) by the same spectral tools experienced in the current study.

Generally, fluoride glasses are characterized by their low dispersion and small non-linear refractive index which may be attractive for handling high laser power density [20]. In addition, they are stable in the ambient atmosphere as long as condensation of water is prevented. Obviously, the previous features lead to conducting studies for improving the optical behavior of fluoride glasses.

A current study by Espinosa-Cerón et al. [21] has reached the conclusion that the Nd^{3+} ions possess spectral properties to be recommended for near-infrared laser applications and further studies are needed to confirm this assumption.

The main objective of the study is to evaluate the building structure and optical properties Nd^{3+} -doped fluoroborate host glasses. In addition to the optical properties, theoretical model Judd–Ofelt (J–O) calculations are carried out to account for the radiative parameters and NIR-photoluminescence efficiency of the Nd^{3+} ion in the present glass matrix.

2 Experimental details

2.1 Materials and preparation of the glasses

About 20 gm of glasses of the chemical composition 70B_2O_3–25NaF–5La$_2$O$_3$–xNd$_2$O$_3$ in mol% (where $x = 0$, 0.05,0.1, and 0.2) were prepared by melting the weighed batches from laboratory chemicals (with purity 99.9%) in platinum crucibles at 1100 °C for 90 min in SiC heated furnace (Vecstar, UK). The chemicals used include orthoboric acid (H_3BO_3) and sodium fluoride (NaF), lanthanum oxide (La$_2$O$_3$), and a dopant of neodymium oxide (Nd$_2$O$_3$). After complete melting, the homogeneous melts were poured into preheated stainless steel molds with the required dimensions. The prepared glassy samples were immediately transferred to an annealing muffle furnace regulated at 300 °C to avoid the thermal stress of glass caused by quenching. The muffle was switched after 1 h and left to cool to room temperature at a rate of 30 °C/h with the glass samples inside.

The density of the glass samples was determined by the standard Archimedes principle using a sensitive balance and xylene as an inert immersion liquid. The density (listed in Table 1) of undoped and Nd$_2$O$_3$-doped glasses was obtained from the relation $\rho = (a/a–b)\,\rho_x$ where a is the weight of the glass sample in air, b is the weight of the glass sample when immersed in xylene of density (ρ_x) 0.865 g/cm^3.

2.2 Techniques for property measurements

2.2.1 Optical absorption measurements

The prepared glasses (Table 1) were characterized by measuring their optical (UV–visible) spectra by means of a recording spectrophotometer type (JASCO V-570, Japan) within the range 200–1100 nm.

2.2.2 Photoluminescence measurements

Photoluminescence measurements were recorded at room temperature under the excitation wavelength of 402 nm in the spectral region 500–760 nm using a fluorescence spectrofluorometer (type FS5 Edinburgh, England) equipped with a light source of Xenon arc lamp 150 W as an excitation light source.

On the basis of the Judd–Ofelt theory, the f–f intensity and transitions can be estimated using the following standard relations [22–24]

From the absorption spectra, the experimental oscillator strength (f_{exp}) for a transition definitely starting from a Ln^{3+} ion's ground state can be calculated according to the following formula:

$$f_{exp} = 4.318 \times 10^{-9} \int \varepsilon(v)dv \tag{1}$$

where ε is the molar extinction coefficient at average energy v cm^{-1}.

$$f_{cal} = \left[8\pi^2 mcv/3h(2J+1)\right]\left[(n^2+2)^2/9n\right] \sum_{\lambda=2,4,6} \Omega(\psi J \parallel U^\lambda \parallel \psi' J')^2 \tag{2}$$

Table 1 Chemical composition of the prepared glasses in mol%

Sample	B_2O_3	NaF	La$_2$O$_3$	Nd$_2$O$_3$	Density (g/cm^3)
1	70	25	5	0	2.608
2	70	25	5	0.05	2.621
3	70	25	5	0.1	2.643
4	70	25	5	0.2	2.658

A transition between two multiplets of an electric dipole's oscillator strength, f, is given by the f–f intensity model of the JO theory. Therefore, from the ground state to an excited state, the predicted oscillator strength is given by

$$S_{ed} = e^2 \sum_{\lambda=2,4,6} \Omega(\psi J \parallel U^\lambda \parallel \psi' J')^2 \tag{3}$$

$$S_{md} = (e^2 h^2 / 16\pi^2 mc^2)(\psi J \parallel L + 2S \parallel \psi' J')^2 \tag{4}$$

where m equals the electron mass, c the velocity of light in vacuum, h the Planck's constant, n the refractive index of the medium, J the total angular momentum of the initial state, v the mean energy of the transition in cm^{-1} and Ω_λ ($\lambda = 2,4,6$) the JO intensity parameters and $\|U^\lambda\|^2$ the squared doubly reduced matrix elements of the unit tensor operator of the rank = 2, 4, and 6 which are calculated from the intermediate coupling approximation for a transition $\psi J \rightarrow \psi' J'$. The oscillator strengths of the observed transitions can be estimated from Eq. 2 to calculate Ω_λ parameters by a standard least-square fitting method. Through the JO theory, the electric and magnetic dipole line strengths for a transition from a level ψJ to a level $\psi' J'$ can be estimated from;

$$A(\psi J, \psi' J') = A_{ed} + A_{md} \tag{5}$$

Using S_{ed} and S_{md}, the radiative transition probability (A) for a transition $\psi J \rightarrow \psi' J'$ can be calculated from the relation;

$$A_{ed} = [64\pi^4 v^3 / 3h(2J+1)][(n^2+2)^2/9n]S_{ed} \tag{6}$$

$$A_{md} = [64\pi^4 v^3 / 3h(2J+1)]n^3 S_{md} \tag{7}$$

where A_{ed} and A_{md} are the electric and magnetic dipole radiative transition probabilities, respectively, given by

$$A_T(\psi J) = \sum_{\psi' J'} A(\psi J, \psi' J') \tag{8}$$

The total radiative transition probability (A_T) for an excited state is given as the sum of the $A(\psi J, \psi' J')$ terms calculated over all the terminal states.

$$\tau_R(\psi J) = [A_T(\psi J)]^{-1} \tag{9}$$

$$\beta_R(\psi J, \psi' J') = A(\psi J, \psi' J')/A_T(\psi J) \tag{10}$$

A_T is related to the radiative lifetime (τ_R) and the branching ratio (β_R) of an excited state by.The peak stimulated emission cross-section, $\sigma(\lambda_P)$, which is essential in predicting the laser performance, is related in terms of the radiative transition probability (A) of a transition as;

$$\sigma(\lambda_P) = (\lambda_P^4 / 8\pi cn^2 \Delta\lambda_{eff})A(\psi J, \psi' J') \tag{11}$$

where λ_P is the average emission transition peak wavelength and $\Delta\lambda_{eff}$ is its effective line width found by dividing the area of the emission band by its average height.

2.2.3 Fourier transform infrared absorption measurements (FTIR)

The FT infrared absorption spectra of the prepared glasses were measured at room temperature using the KBr disc technique on a Fourier transform computerized infrared spectrometer type (FTIR 4600 JASCO Corp Japan). The glasses were tested in the form of a crushed powder that was combined with KBr at a 1:100 mg glass powder to KBr ratio. The weighed mixes were then exposed to a 5-ton/cm^2 pressure to yield clear homogenous discs.

3 Results and discussion

3.1 Optical absorption spectra

Figure 1 illustrates the UV–visible spectra of the base undoped glass and also that for samples doped with 0.05, 0.1, or 0.2% Nd_2O_3. The base glass without Nd_2O_3 reveals a spectrum consisting of two distinct UV absorption bands at 223 nm and at 280 nm with the first band with higher intensity than the second band and without any further absorption to the end of measurements.

The glasses containing dopants of Nd_2O_3 show beside the mentioned UV-bands as the undoped glass, distinct and extended absorption extending from 430 to 875 nm. The identified 10 absorption bands are observed at 431, 472, 511,
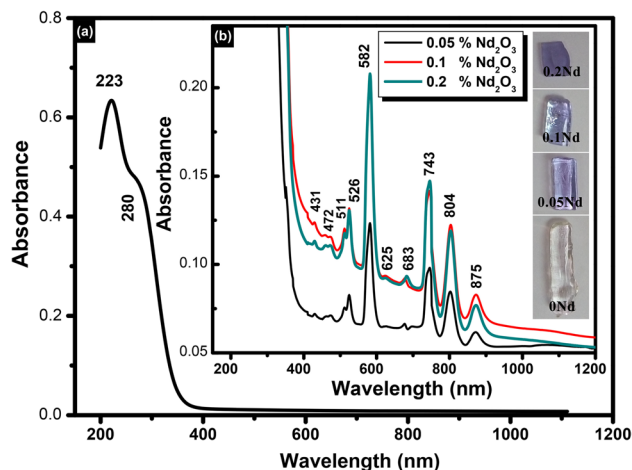

Fig. 1 Optical absorption spectra of **a** undoped and **b** Nd_2O_3-doped sodium fluoroborate glass
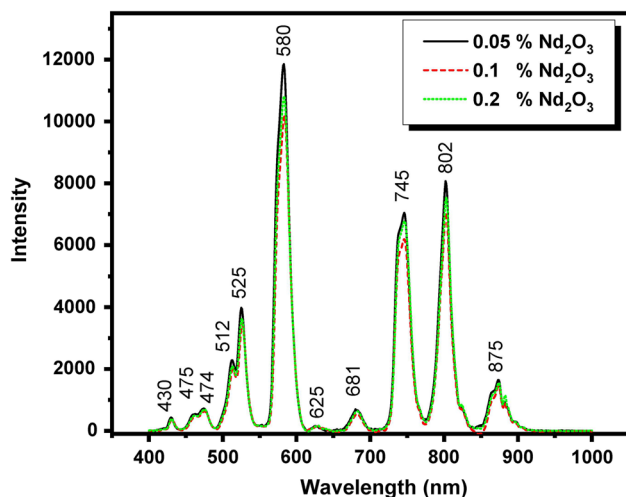
526, 582, 625, 683, 743, 804 and 875 nm. The three bands at 582, 743, and 804 are distinctly more intense than the others but decrease in intensity with the increase of wavelength. On the other hand, the intensities of all the absorption bands identified are generally observed to increase with the increase of Nd_2O_3 content. The identified spectra indicate that the Nd^{3+}-containing glasses display characteristic bands which are repetitive and quite different than that for the parent undoped glass. The identified two UV absorption bands from the spectrum of the undoped glass are attributed to originate from unavoidable trace ferric ions present as impurities (even in ppm) in the laboratory chemicals used for the preparation of the glasses and agree with the assumption of many glass scientists who identified and characterize UV absorption in many undoped glasses [16–18, 25–28].

The various extended bands identified within the spectra of Nd_2O_3-doped glasses are related to the following transitions [8, 17, 18]:

(1) 431 nm($^2P_{1/2}$), (2) 472 nm($^2G_{9/2}$), (3) 511 nm($^4G_{9/2}$), (4) 526 nm($^4G_{7/2}$), (5) 582 nm($^4g_{5/2}$), (6) 625 nm($^2H_{11/2}$), (7) 683 nm($^4F_{9/2}$), (8) 743 nm($^4S_{3/2} + 4F_{5/2}$), (9) 804 nm($4F_{5/2}$), (10), and 875($^4F_{3/2}$). These described bands were previously identified by referring to their energies as shown by Carnal et al. [29] and to that reported by other authors [27, 28]. The increase in absorbance intensity with an increase in the doping can be related to the increase of Nd^{3+} ions as color centers.

3.2 Photoluminescence spectral data

Figure 2 displays the excitation spectra of the three doped Nd_2O_3 glasses (0.05, 0.1, 0.2% Nd_2O_3). The excitation spectra are identified to comprise 11 peaks owing to the quantum transition from a lower energy state to an excited state. The excitation peaks correspond to 430 nm, 455 nm, 474 nm, 512 nm, 525 nm, 586 nm, 625 nm, 681 nm, 745, 802 nm, 875 nm [30–33]. It is identified that the peak at 580 nm is the most prominent among all peaks and which is chosen as an excitation wavelength specific for measurements of emission spectra.

Figure 3 illustrates the emission spectra after excitation at (580 nm) of Nd_2O_3-doped glasses. The collected emission spectra show three distinct bands at 875 nm ($^4F_{3/2} \rightarrow {}^4I_{9/2}$), 1056 nm ($^4F_{3/2} \rightarrow {}^4I_{11/2}$) and 1326 nm ($^4F_{3/2} \rightarrow {}^4I_{3/2}$) which are attributed to Nd^{3+} ions transitions. The emission spectrum demonstrates that the emission intensity decreases with the increase of Nd_2O_3 content from 0.05 to 0.1% Nd_2O_3 and then returns to its previous intensity with the increase of Nd_2O_3 to 0.2%. This phenomenon is known as luminescence quenching. This means that the intensity of emission spectra depends on the number of active centers.

It is assumed that the density or concentration effect of Nd^{3+} ions rises with the increase of doping and with the rise of the concentration of Nd^{3+} ions, the intramolecular gap decreases and the Nd^{3+} ions are very closed resulting in a significant interaction between the dopant ions. Thus, there is an effective transfer of energy among Nd^{3+} ions which leads to luminescence quenching. These findings are consistent with previous studies [27, 28].

Ramteke et al. [32] studied optical and photoluminescence spectra of Nd^{3+} in lithium borate glasses and showed that optical spectra are due to Nd^{3+} ions and the luminescence intensity was maximum at 1% Nd_2O_3 and a further increase in Nd_2O_3 resulted in luminescence quenching. They attributed this quenching behavior to the Nd^{3+}–Nd^{3+} interaction in the glass matrix. The results and attribution are in good agreement with previously reported results [33]. Kaewnum et al. [34] studied the luminescence properties of Nd^{3+}

Fig. 2 Excitation spectra of Nd_2O_3-doped sodium fluoroborate glass at $\lambda_{em} = 1056$ nm
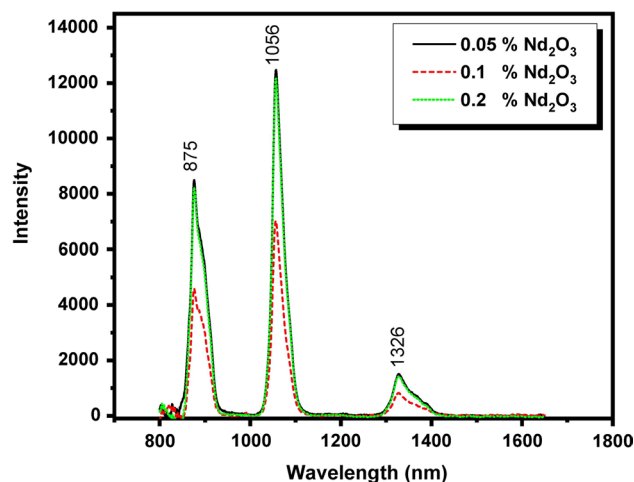
Fig. 3 Emission spectra of Nd_2O_3-doped sodium fluoroborate glass at $\lambda_{ex} = 580$ nm

doped lithium lanthanum borate glass and made Judd–Ofelt analysis and concluded that this glass can be used as a laser medium in a glass emitting laser device.

Recently a study by Aljewaw et al. [35] on Li–Al–borate glass with varying Nd_2O_3 contents has reached the nomination of this glass system for diverse applications such as laser application and radiation dosimetry.

3.3 Judd–Ofelt analysis and radiative parameters

The analysis of the Judd–Ofelt parameters was performed using the oscillator strengths of the recorded transitions in the $Nd^{3+}4f$ quantum states. The experimental f_{exp} and calculated oscillator strength f_{cal} values of the prepared Nd_2O_3-doped glasses are listed in Table 2 adopting the root mean square error (RMS) deviation. According to Yaacob et al. [36], the oscillator strength values are an indication of the environmental symmetry around the rare earth in the glass network, and they refer to conclude that lower oscillator strength values indicate a highly symmetrical rare earth environment, whereas high oscillator strength values indicate that the glass is asymmetry and the ligands are covalently bonded. As observed from Fig. 2 the most intensive peak is located at 580 nm which is assigned to $^2G_{7/2} + {}^4G_{5/2}$ electronic transitions and denoted by the hypersensitive transition (HST). The decrement in the RMS values indicated that the agreement between the calculated and experimental values and the considerable reduction in oscillator strength could be attributed to enhancing site symmetry around the Nd^{3+} ion and decreased covalent character of the bonds [36, 37].

The estimated Judd–Ofelt parameters Ω_2, Ω_4, and Ω_6 of Nd_2O_3-doped glasses are given in Table 3. According to the recorded values in the table, the intensity trend of parameters is varied with Nd_2O_3 content and has been found to be $\Omega_6 > \Omega_2 > \Omega_4$ for 2N sample, $\Omega_2 > \Omega_6 > \Omega_4$ for 3N sample, and $\Omega_6 > \Omega_2 > \Omega_4$ for 4N sample. The intensity parameter Ω_6

Table 3 Judd–Ofelt parameters $\Omega_{2, 4, 6}$ ($\times 10^{-20}$ cm²) for the Nd-doped borate glasses

Sample	Ω_2	Ω_4	Ω_6
2N	14.78	8.76	15.18
3N	8.57	2.36	8.56
4N	2.37	0.62	2.57

is assumed to be closely related to the local structure of the rare earth ions and the covalency degree Nd–O bonds while Ω_2 and Ω_4 parameters are strongly affected by the toughness and viscosity of the glass matrix and the greater Ω_6 in the current glass indicates its rigidity, while the lower Ω_2 suggests increased asymmetry and less covalency between the Nd–O group in 4N glass [36–39].

The literature indicates that JO characteristics are typically correlated with the covalency between RE ions and ligand anions as well as the local environment's asymmetries at the site of RE ions. Therefore, as the JO parameters increase, the ion site becomes less centrosymmetric and the chemical interactions between the ligands become more covalent [40, 41]. Additionally, the increase in 2, 6 values show a more distorted local structure at the Nd^{3+} ions sites, which may be caused by increased polymerization of the glass dominant network and a higher covalency of the Nd–O bond in the current glassy system [41].

Numerous studies [41–43] have indicated that any observable shift of peak wavelength of the fluorescence spectrum of Nd^{3+} ion to a longer wavelength was caused by the increase of the covalency between the Nd^{3+} and the oxygen in oxide glasses. Hence, for glasses, the Judd–Ofelt parameters are related to the local structure in the vicinity of rare earth ions and/or the covalency of rare earth ions sites. For instance, the transition whose intensity is determined mainly by the $\Omega_2 < \| U^{(2)} \| > ^2$ term, called the hypersensitive transition, is sensitive to the local structures in the vicinity of the rare–earth ions relating to the anion

Table 2 The experimental and calculated oscillator strengths ($\times 10^{-6}$) for Nd-doped borate glasses

Wavelength (nm)	Energy level	Sample (2N)		(Sample 3N)		Sample 4N	
		P_{exp}	P_{calc}	P_{exp}	P_{calc}	P_{exp}	P_{calc}
431	$^2P_{1/2}$	1.7753	1.0987	0.4604	0.3043	0.2261	0.0848
468	$^4G_{11/2} + ({}^2D, {}^2P)_{3/2} + {}^2G_{9/2} + {}^2K_{15/2}$	3.9124	3.0040	2.5246	1.3767	0.6916	0.4233
520	$^4G_{9/2} + {}^4G_{7/2} + {}^2K_{13/2}$	20.9031	13.6782	9.6471	6.3332	2.8863	1.9117
581	$^2G_{7/2} + {}^4G_{5/2}$	60.0229	52.0249	30.8403	26.5165	8.8883	7.6636
630	$^2H_{11/2}$	0.4343	0.4319	0.1538	0.2369	0.0604	0.0743
683	$^4F_{9/2}$	1.0213	1.5976	0.8460	0.8866	0.1330	0.2785
744	$^4S_{3/2} + {}^4F_{7/2}$	25.9072	20.9221	15.1764	11.9802	4.7341	3.7566
805	$^2H_{9/2} + {}^4F_{5/2}$	19.6908	18.8758	10.0979	9.8392	3.0873	3.0438
877	$^4F_{3/2}$	5.9750	4.9252	2.9065	1.8140	0.8083	0.5099
	RMS	4.90581×10^{-6}		2.66157×10^{-6}		0.775602×10^{-6}	

structures of the host glasses while the other hand, the intensity parameters Ω_4 and Ω_6 are insensitive to the local structures but related to the covalency of the rare–earth ion sites in silicate, borate, and phosphate glasses [40–43]. As for alkali-containing glasses, when the rare earth ion is incorporated into the anion network oxide glasses as a modifier, the RE^{3+}, modifying cations and NBO's probably form depolymerized regions throughout the network resulting in the variations of the covalency of the rare earth – ion sites, which proceeds from an increase in the ionic packing ration, caused by changing the type of the alkali ion [40–43].

On the other hand, from the Judd–Ofelt theory, the line strength $S_{cal}(J \rightarrow J')$ between the initial state J characterized by (S, L, J) and the final state J' given by (S', L', J') has been estimated. Hence, Table 4 introduces the values of radiative probabilities A (s^{-1}), branching ratio (β_R), and the radiative lifetime (τ_R) for the transitions $^4F_{3/2} \rightarrow {}^4I_{15/2}$, $^4F_{3/2} \rightarrow {}^4I_{13/2}$, $^4F_{3/2} \rightarrow {}^4I_{11/2}$, $^4F_{3/2} \rightarrow {}^4I_{9/2}$ and their correlation to the Nd_2O_3 content. The decrease in radiative transition probability can be attributed to rare-earth ion (Nd^{3+}) accumulation and coupling with the phonon lattice vibration and through the phonon-electron interaction, the excited electron is most likely transferred to the phonon subsystem and releases some energy in the form of heat [37]. In the same context, the branching ratio (β_R) data indicated the ability to increase particularly stimulated emission transitions. The results show that the maximum value of the branching ratio is corresponding to $^4F_{3/2} \rightarrow {}^4I_{11/2}$ transition, hence the most prospective emission with high intensity occurs due to $^4F_{3/2} \rightarrow {}^4I_{11/2}$ transition. The obtained results are matched with that obtained and also suggested by previous study [36]. The trend of a lifetime is observed to be increased with increasing the Nd_2O_3 content.

The emission band positions, effective bandwidths and the stimulated emission cross-sections for Nd-doped borate glasses are listed in Tables 4 and 5. It can be assumed that under excitation at 580 nm, the electrons are absorbed and transferred from the highest energy levels to the most stable energy level $^4F_{3/2}$ as a result of the non-radiative relaxation. The emission of photons mainly depends on the allowed transitions from the relations process that induced $^4F_{3/2} \rightarrow {}^4I_{9/2}$, $^4F_{3/2} \rightarrow {}^4I_{11/2}$ and $^4F_{3/2} \rightarrow {}^4I_{13/2}$ transitions. According to data listed in Table 5 the largest stimulated emission cross-section is for the transition $^4F_{3/2}$ to $^4I_{11/2}$ and also is observed in glass with 0.05 mol% Nd_2O_3, which is higher than that with other listed glasses. It was reported by many previous studies [44–46], that materials used in the development of solid-state lasers should have a high effective emission cross-section to produce maximum photon emissions. The represented data indicated that the transition line $^4F_{3/2} \rightarrow {}^4I_{11/2}$ is the sharpest and lowest bandwidth value than other detected transitions, making it more appropriate for laser applications as suggested by previous assumption [44–46]. The bandwidth gain value is a predictive tool for the amplification of the laser glass, hence glasses with high gain bandwidth can be applied to operate the continuous wave laser directly that depends mainly on the host material, emission cross section and the duration of the excited level [44–46].

Fluoroborate glasses typically offer the best overall mix of properties for many different laser applications, but rarely exhibiting the extreme property values achievable when compared to other glasses. The number of commercially accessible laser glasses is extremely tiny in compared to the vast array and variety of glasses evaluated spectroscopically [8]. Large, regular variations in the Judd–Ofelt parameters with glass type and composition

Table 4 Radiative (A) and total radiative (A_T) transition probabilities, branching ratio (β_R) and lifetime (τ_R) for emission levels of Nd-doped borate glasses

SLJ	S'L'J'	ν (cm^{-1})	2N		3N		4N	
			A (s^{-1})	β_R	A (s^{-1})	β_R	A (s^{-1})	β_R
$^4F_{3/2}$	$^4I_{15/2}$	5405	42.6311	0.0060	23.3549	0.0071	7.7092	0.0073
	$^4I_{13/2}$	7541	838.1583	0.1171	459.1744	0.1405	151.5680	0.1438
	$^4I_{11/2}$	9470	3788.2083	0.5293	1925.9670	0.5894	630.0288	0.5979
	$^4I_{9/2}$	11,236	2488.0089	0.3476	859.4458	0.2630	264.4408	0.2510
	A_T (s^{-1})		7157.0066		3267.9421		1053.7468	
	τ_R (µs)		0.0001397		0.0003060		0.0009490	

Table 5 Emission band positions (λ_p, nm), effective bandwidths ($\Delta\lambda_{eff}$, nm) and stimulated emission cross-sections ($\sigma(\lambda_p) \times 10^{-20}$ cm^2) for Nd-doped borate glasses

Transition $^4F_{3/2}\rightarrow$	2N			3N			4N		
	λ_p	$\Delta\lambda_{eff}$	$\sigma(\lambda_p)$	λ_p	$\Delta\lambda_{eff}$	$\sigma(\lambda_p)$	λ_p	$\Delta\lambda_{eff}$	$\sigma(\lambda_p)$
$^4I_{13/2}$	1326	53.055	2.5230	1326	49.600	1.5886	1326	48.470	0.5067
$^4I_{11/2}$	1056	32.166	7.8937	1056	31.580	4.2096	1056	31.900	1.2872
$^4I_{9/2}$	885	37.177	1.9615	885	38.300	0.7641	885	37.010	0.2297

have been found for lanthanide ions based on knowledge of these fluctuations. Comparing the spectra in the current study, the $^4F_{3/2} \rightarrow ^4I_{11/2}$ fluorescence of Nd-doped fluoroborate glass is more intensive than that for the other glasses [14, 16–18]. In contrast, to multicomponent silicate, phosphate, or other oxide or halide glasses, simple fluoroborate glasses show a higher degree of covalent bonding of Nd^{3+}. The second attribute indicates a stronger local field strength and/or more site-to-site changes in the field. The examined glass has an acceptable optical quality that is within bounds and can satisfy the requirements of lasing applications.

3.4 FT infrared absorption spectra of the prepared glasses

Figure 4a and b illustrate the deconvoluted IR spectra of both the undoped glass and 0.2% Nd₂O₃-doped glass. The curve fitting of IR absorption spectra is a useful technique that can be used to facilitate data interpretation. In curve fitting, the experimental spectrum is modeled as a sum of individual spectral contributions.

The measured IR spectrum of the undoped glass reveals distinct and extended far-IR peaks from 400 to about 600 cm^{-1} and ended by an attached small band at about 650 cm^{-1}. The rest of the IR spectrum comprises a first very broad band extending from 800 to 1200 cm^{-1} and revealing two bands, a medium band at about 900 cm^{-1} and a high intense band with a peak at about 1020 cm^{-1}. A further second broad band is identified to be extending from 1200 to 1650 cm^{-1} with a high intense band with a peak at about 1416 cm^{-1} and followed by an attached medium band at 1600 cm^{-1}. The inside spectrum of the undoped glass (Fig. 4a) reveals extended absorption peaks at 413, 497, 557, 651, 897, 1020, 1104, 1416, 1487, and 1635 cm^{-1}.

The IR spectrum of the 0.2% Nd₂O₃-doped glass shows an intense far-IR broad band centered at about 469 cm^{-1} and followed by a very broad band with higher intensity and extending from about 800–1200 cm^{-1} and revealing a medium band at about 900 cm^{-1} and a high intense band with a peak at about 1020 cm^{-1}. A further second broad and distinct band is identified extending from 1200 to 1650 cm^{-1} with a band at about 1400 cm^{-1} and followed by an attached medium band at 1600 cm^{-1}. The inside spectrum of the undoped glass (Fig. 4a) reveals extended absorption peaks at 413, 497, 557, 651, 897, 1020, 1104, 1416, 1487 and 1635 cm^{-1}.

The spectrum of the 0.2 Nd₂O₃-doped glass reveals extended deconvoluted peaks at 402, 461, 550, 635, 910, 1021, 1105, 1401, 1615 and 1660 cm^{-1}.

The details of the FTIR vibrational modes and their assignments are listed in Table 6.
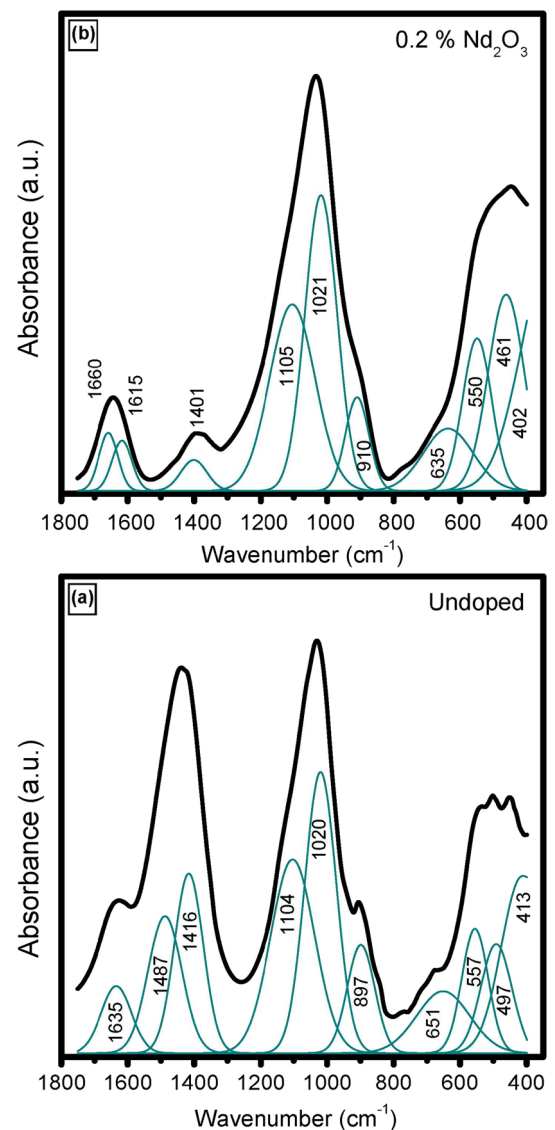
Fig. 4 FTIR absorption spectra of **a** undoped glass and **b** 0.2%Nd₂O₃-doped sodium fluoroborate glass

The understanding and interpretations of the identified IR spectral peaks from the undoped fluoroborate glass are based on the following basis [3, 47–57]:

(a) It is agreed that the identified IR absorption bands are originating from vibrations of the structural building units or fingerprints of them within the studied glasses which depend on the detailed chemical composition of the glass constituents and the expected structural groups formed.

(b) The chemical composition of the base host glass consists of main 70% B_2O_3, 25% NaF and 5% La_2O_3.

(c) It is recognized that alkali and alkaline earth fluorides behave in a similar way as the corresponding oxides.

Table 6 Infrared absorption spectra and their assignment

Peak position	Assignment	References
402–497	La^{3+} vibrational modes of LaO_6 or Nd–O vibrational modes	[51–53]
550–560	Vibration due to metal cation Na^+ and La^{3+}	[52–54]
635–650	B–O–B bending vibrations in symmetric BO_3 triangles	[12, 55]
897–910	the B–O symmetric stretching vibration of BO_4 tetrahedral units	[55]
1020	Pentaborate group or asymmetric stretching modes of BO_4 vibrations attached with the non-bridging oxygen in the borate network	[56, 57]
1105	Asymmetric stretching of BO_4 units in the BO_4–O linkages	[12, 56, 57]
1400–1487	B–O asymmetric stretching vibrations of BO_3 units from metaborate, pyroborate and orthoborate groups	[12, 52–57]
1615–1660	Asymmetric stretching relaxation of B–O bonds of trigonal BO_3 units	[12, 56]

Alkali fluorides are assumed to progressively convert some of the initial structural BO_3 groups in (B_2O_3) to be changed to (BO_3F) groups in a similar behavior to the formation of tetrahedral (BO_4) with alkali oxides. This conversion process proceeds to a certain limit which is characteristic to each alkali fluoride and the excess of the alkali fluoride is assumed to form additional tetrahedral alkali fluoride groups or units (e.g., NaF_4) and not to form nonbridging oxygens as with alkali oxide.

(d) The confirmation of the previous assumption can be realized by referring to the intensities of the IR bands. It is accepted that the triangular BO_3 groups are vibrating within the range of 1200–1600 cm^{-1} while the tetrahedral (BO_3F) groups are vibrating within the range 800–1200 cm^{-1}. The high intensities of the IR bands within the range 800–1200 cm^{-1} refer to the assumption that it is assumed to originate from the combination mode of vibrations of tetrahedral (BO_3F) and (NaF_4) groups [7, 48].

(e) The identified changes upon the increase of Nd_2O_3 content on the IR spectra (Fig. b) can be attributed to any or all of the following reasons [3, 7, 50]:

(f) Suggested depolymerization effects causing the extension of the IR vibrational bands due to (BO_3) groups or derivatives group to extend from 1200 to 1650 cm^{-1} with different distributions including the appearance of vibrational bands at 1401, 1615 and 1660 cm^{-1}, accompanied by the observed decrease of the band at 1416 cm^{-1} in the undoped glass (Fig. 4a).

(g) The assumption that Nd_2O_3 can cause the transformation of some structural B–O bonds within the range of triangular borate units such as the formation of pyroborate units or similar structural groups.

There is also a characteristic limit of the maximum concentration of $[BO_4]$ structural groups. If it exceeds the maximum concentration, the reconversion of $[BO_4]$—units to $[BO_3]$—and $[BO_3]$—units (boron with one and two nonbridging oxygen atoms) would have been occurred. The creation of non-bridging oxygen atoms would leads to the disappearance or shift in the position of absorption bands [51]. Obviously, the addition of Nd_2O_3 causes some changes in the structural building units and due to loosely connected linkage or units of the bridging oxygen from network building units (BO_3/BO_4) cause a change in the shape and the position of the absorption bands to the higher wave number.

4 Conclusion

A novel host fluoroborate glass of chemical composition 70%B_2O_3–25% NaF–5 La_2O_3 together with Nd_2O_3-doped samples was prepared via melting and annealing technique. The undoped glasses reveal two UV absorption peaks at 223 nm and 280 nm that related to traces of ferric iron impurities. Nd_2O_3-doped glass show beside the UV-peaks as the undoped glass distinct extended absorption peaks from 430 to 875 nm with identified 10 absorption peaks at about 431($^2P_{1/2}$), 472 ($^2G_{9/2}$), 511($^4G_{9/2}$), 526 ($^4G_{7/2}$), 582 ($^4g_{5/2}$), 625 ($^2H_{11/2}$), 683($^4F_{9/2}$), 743 ($^4S_{3/2} + 4F_{5/2}$), 804 ($4F_{5/2}$) and 875 nm ($^4F_{3/2}$). The emission after excitation at (580 nm) of Nd_2O_3-doped glasses spectrum shows three distinct bands at 875 nm ($^4F_{3/2} \rightarrow {}^4I_{9/2}$), 1056 nm ($^4F_{3/2} \rightarrow {}^4I_{11/2}$) and 1326 nm ($^4F_{3/2} \rightarrow {}^4I_{3/2}$) which are attributed to Nd^{3+} ions transitions. The emission spectrum shows that the intensity of the emission reduces as Nd_2O_3 content rises from 0.05 to 0.1% and then returns to its initial intensity when Nd_2O_3 rises to 0.2%. The intensity trend of the parameters varies with Nd_2O_3 content and has been found to be $\Omega_6 > \Omega_2 > \Omega_4$ for the 2N sample, $\Omega_2 > \Omega_6 > \Omega_4$ for the 3N sample, and $\Omega_6 > \Omega_2 > \Omega_4$ for 4N sample. The analysis of the Judd–Ofelt parameters indicates that the most intense peak is located at 580 nm and is assigned to $^2G_{7/2} + {}^4G_{5/2}$ electronic transitions. The Ω_2 and Ω_4 intensity parameters are strongly influenced by the toughness and viscosity of the glass matrix, and the maximum value of the branching ratio is corresponding to the $^4F_{3/2} \rightarrow {}^4I_{11/2}$ transition, the most prospective emission with

high intensity occurs as a result of the $^4F_{3/2} \rightarrow {}^4I_{11/2}$ transition. The intensity parameter Ω_6 is assumed to be closely related to the local structure of the rare earth ions and the covalency degree Nd–O bonds. According to FTIR studies, the IR absorption bands in the 800–1200 cm^{-1} range are caused by the combined tetrahedral vibrations of the (BO$_4$), (BO$_3$F), and (NaF$_4$) groups, while the vibrations in the 1200–1600 cm^{-1} range are caused by the triangular (BO$_3$) groups. The presence of Nd$_2$O$_3$ alters some structural B–O bonds in the range of triangular borate units, which may cause depolymerization and the emergence of pyroborate units or other structural groups. The examined Nd$_2$O$_3$-doped B$_2$O$_3$–NaF–La$_2$O$_3$ can be advised to be suited for laser applications, according to the overall measured spectrum features.

Declarations

References

1. A. Paul, *Chemistry of glasses*, 2nd edn. (Elsevier, New York, 1990)
2. J.E. Shelby, *Introduction to glass science and technology*, 2d edn. (The Royal Society of Chemistry, Cambridge, UK, 2005)
3. E. Kamitsos, Infrared studies of borate glasses. Phys. Chem. Glasses **44**, 79–87 (2003)
4. M. Azooz, H.A. ElBatal, Preparation and characterization of invert ZnO-B$_2$O$_3$ glasses and its shielding behavior towards gamma irradiation. Mater. Chem. Phys. **240**, 122129 (2020)
5. K. MacDonald, D. Boyd, Investigation of multicomponent fluoridated borate glasses through a design of mixtures approach. Materials **15**, 6247 (2022)
6. R. Nagaraju, L. Haritha, K.C. Sekhar, Md. Shareefuddin, G. Lalitha, K.V. Kumar, Study of mixed heavy metal fluoride bismuth borate glasses for optical applications. J. Mater. Sci.: Mater. Electron. **33**, 14397–14408 (2022)
7. M.A. Ouis, M.A. Marzouk, F.H. ElBatal, Preparation and characterization of glasses from the binary sodium fluoroborate system NaF–B$_2$O$_3$ within the range (10–50 mol% NaF) assessed by structural FTIR, optical and thermal properties and effects of gamma irradiation. J. Mol. Struct. **1260**, 132881 (2022)
8. M.J. Weber, Science and technology of laser glass. J. Non-Cryst. Solids **123**, 208–202 (1990)
9. I.N. Chakraborty, J.E. Shelby, R.A. Condnrate, Properties and structure of lanthanum borate glasses. J. Amer. Ceram. Soc. **67**, 782–785 (1984)
10. Y.J. Seo, D.J. Shin, Y.S. Chao, Phase evolution and microwave dielectric properties of lanthanum borate-based low-temperature co-fired ceramics materials. J. Amer. Ceram. Society **89**, 2352–2355 (2006)
11. R.S. Gedam, D.D. Ramteke, Electrical, dielectric and optical properties of La$_2$O$_3$ doped lithium borate glasses. J. Phys. Chem. Solids **74**, 1039–1044 (2013)
12. A.V. Deepa, P. Murugasen, S. Sagadevan, A study of the structural, spectroscopic, and dielectric properties of La$_2$O$_3$ doped borate glass. J Mater Sci: Mater Electron. **28**, 10780–10784 (2017)
13. S. Kuretake, N. Tanaka, Y. Kintake, E. Kageyama, H. Nakao, A. Shirakawa, K. Ueda, A.A. Kaminskii, Nd-doped Ba(Zr, Mg, Ta) O$_3$ ceramics as laser materials. Opt. Mater. **36**, 645–649 (2014)
14. N.N. Yusof, S.K. Ghoshal Dr, S.A. Jupri, M.N. Azlan, Nd^{3+} doped magnesium zinc sulfophosphate glass: new candidate for up-conversion solid-state laser host. Opt. Mater. **109**, 110299 (2020)
15. N. Kiwsakunkran, W. Chaiphaksa, N. Chanthima, H.J. Kim, S. Kothan, A. Prasatkhetragarn, Kaewkhao, fabrication of K$_2$O–Al$_2$O$_3$–Gd$_2$O$_3$-P$_2$O$_5$ glasses for photonic and scintillation materials applications. Radiat. Phys. Chem. **188**, 109639 (2021)
16. A. R. Venugopal, R. Rajaramakrishna, K. M. Rajashekara, V. Pattar, N. Wongdamnern, S. Kothan, J. Kaewkhao (2022) Nd^{3+}-doped B$_2$O$_3$ + Li$_2$O + CaO + CaF$_2$ glass systems: Structural and optical properties, 133:112979.
17. D. Ramachari, L.R. Moorthy, C.K. Jayasankar, Optical absorption and emission properties of Nd^{3+}-doped oxyfluorosilicate glasses for solid state lasers. Infrared Phys. Technol. **67**, 555–559 (2014)
18. A. BalaKrishna, D. Rajesh, Y.C. Ratnakaram, Structural and optical properties of Nd^{3+} in lithium fluoro-borate glass with relevant modifier oxides. Opt. Mater. **35**, 2676–2676 (2013)
19. F.H. ElBatal, M.A. Marzouk, H.A. ElBatal, Y.M. Hamdy, Behavior of bismuth ions in the two glassy systems of 50 LiF-50 P$_2$O$_5$ and 50 LiF-50 B$_2$O$_3$ (mol%) assessed by optical, FTIR and photoluminescence spectra in addition to thermal expansion properties. Opt. Quantum Electron. **55**, 217 (2023)
20. M. Poulain, Fluoride glasses: properties, technology and applications, in *Photonic Glasses and Glass-Ceramics*. ed. by G.S. Murugan (Research Signpost, Kerala, 2010), pp.1–28
21. M.Y. Espinosa-Cerón, O. Soriano-Romero, U. Caldiño, R. Lozada-Morales, A.N. Meza Rocha, Spectroscopy evaluation of Nd3+-activated novel CdO–V$_2$O$_5$–ZnO–B$_2$O$_3$ inverted glasses for near infrared laser applications. Ceram. Int. (2023). https://doi.org/10.1016/j.ceramint.2023.05.062
22. C. Gorller-Walrand, K. Binnemans, Spectral intensities of f–f transition, in *Handbook on the Physics and Chemistry of Rare Earths*, vol. 25, ed. by K.H. Gschneidner Jr., L. Eyring (North-Holland, Amsterdam, 1998)

23. P. Balaji, R.R. Abdul Azeem, Reddy, absorption and emission properties of Eu^{3+} ions in sodium fluoroborate glasses. Physica B **394**, 62–68 (2007)

24. E.A. Lalla, M. Konstantinidis, I. De Souza, M.G. Daly, I.R. Martín, V. Lavín, U.R. Rodríguez-Mendoza, Judd–Ofelt parameters of RE^{3+}-doped fluorotellurite glass (RE^{3+}-Pr^{3+}, Nd^{3+}, Sm^{3+}, Tb^{3+}, Dy^{3+}, Ho^{3+}, Er^{3+}, and Tm^{3+}). J. Alloy. Compd. **845**, 156028 (2020)

25. J.A. Duffy, Charge transfer spectra of metal ions in glass. Phys. Chem. Glasses **38**, 289–294 (1997)

26. D. Möncke, D. Ehrt, Irradiation induced defects in glasses resulting in the photoionization of polyvalent dopants. Opt. Mater **25**, 425 (2004)

27. F.H. ElBatal, M.A. Marzouk, A.M. Abdelghany, UV–visible and infrared absorption spectra of gamma irradiated V_2O_5-doped in sodium phosphate, lead phosphate, zinc phosphate glasses: a comparative study. J. Non-Cryst. Solids **357**, 1027–1036 (2011)

28. M.A. Marzouk, Y.M. Hamdy, H.A. ElBatal, F.M. EzzElDin, Photoluminescence and spectroscopic dependence of fluorophosphate glasses on samarium ions concentration and the induced defects by gamma irradiation. J. Lumin. **166**, 295–303 (2015)

29. W.T. Carnall, P.R. Fields, K. Rajnak, Electronic energy levels in the trivalent lanthanide aquo ions. I. Pr^{3+}, Nd^{3+}, Pm^{3+}, Sm^{3+}, Dy^{3+}, Ho^{3+}, Er^{3+}, and Tm^{3+}. J. Chem. Phys. **49**, 4424 (1968)

30. A.D. Sontakke, K. Annapurna, Spectroscopic properties and concentration effects on luminescence behavior of Nd^{3+} doped Zinc–Boro–Bismuthate glasses. Mater. Chem. Glasses **137**, 916–921 (2013)

31. V.Y. Ganvir, H.V. Ganvir, R.S. Gedam, Physical and optical study of Nd_2O_3 doped sodium borosilicate glasses. Mater. Today: Proc. **51**, 1201–1205 (2022)

32. D.D. Ramteke, K. Annapurna, V.K. Deshpande, R.S. Gedam, Effect of Nd^{3+} on spectroscopic properties of lithium borate glasses. J. Rare Earths **32**, 1148–1153 (2014)

33. A.D. Sontakke, K. Biswas, A.K. Mandal, K. Annapurna, Concentration quenched luminescence and energy transfer analysis of Nd^{3+} ion doped Ba-Al-metaphosphate laser glasses. Appl. Phys. B **101**, 235 (2010)

34. E. Kaewnum, N. Wantana, J. Kaewkhao, Luminescence study and Judd–Ofelt analysis of Nd^{3+} doped lithium lanthanum borate glass for green laser device. Mater. Today: Proc. **5**, 13954–13962 (2018)

35. O.B. Aljewaw, M.K. Abdul Karim, H.M. Kamari, M.H.M. Zaid, A.A. Salim, M.H. Abu Mhareb, Physical and spectroscopic characteristics of lithium-aluminium-borate glass: effects of varying Nd_2O_3 doping contents. J. Non-Cryst. Solids **575**, 121214 (2022)

36. S.N.S. Yaacob, M.R. Sahar, F. Mohd-Noor, W.N.W. Shamsuri, S.KMd. Zain, N.A.M. Jan, M.F. Omar, S.A. Jupri, S.M. Aziz, A.S. Alqarni, The effect of Nd_2O_3 content on the properties and structure of Nd^{3+} doped TeO_2–MgO–Na_2O- glass. Opt. Mater. **111**, 110588 (2021)

37. S.K.K. Ghoshal, A. Awang, M.R.R. Sahar, R. Arifin, R. Ari, Gold nanoparticles assisted surface enhanced Raman scattering and luminescence of Er^{3+} doped zinc sodium tellurite glass. J. Alloys Compd **159**, 265–273 (2015)

38. B. Charfi, K. Damak, M.S. Alqahtani, K.I. Hussein, A.M. Alshehri, N. Elkhoshkhany, A.L. Assiri, K.F. Alshehri, M. Reben, E. Yousef, Luminescence and gamma spectroscopy of phosphate glass doped with Nd^{3+}/Yb^{3+} and their multifunctional applications. Photonics **9**, 406 (2022)

39. L.R. Moorthy, T.S. Rao, M. Jayasimhadri, A. Radhapathy, D.V.R. Murthy, Spectroscopic investigations of Nd^{3+}-doped alkali chloroborophosphate glasses. Spectrochim Acta Part A **60**, 2449–2458 (2004)

40. E.O. Serqueira, N.O. Dantas, M.J.V. Bell, Control of spectroscopic fluorescence parameters of Nd^{3+} ions as a function of concentration in a SiO_2–Na_2O–Al_2O_3–B_2O_3 glass system. Chem. Phys. Lett. **508**, 125–129 (2011)

41. Z.A.S. Mahraz, E.S. Sazali, M.R. Sahar, N.U. Amran, S.N.S. Yaacob, S.M. Aziz, S.Q. Mawlud, F.M. Noor, A.N. Harun, Spectroscopic investigations of near-infrared emission from Nd^{3+}-doped zinc-phosphate glasses: Judd–Ofelt evaluation. J. Non-Cryst. Solids **509**, 106–114 (2019)

42. A. Quintas, O. Majerus, M. Lenoir, D. Caurant, K. Klementiev, A. Webb, Effect of alkali and alkaline-earth cations on the neodymium environment in a rare-earth rich aluminoborosilicate glass. J. Non-Cryst. Solids **354**, 98–104 (2008)

43. H. Takebe, Y. Nageno, K. Morinaga, Compositional dependence of Judd–Ofelt parameters in silicate, borate, and phosphate glasses. J. Am. Ceram. Soc. **78**(5), 1161–1168 (1995)

44. Z. Zhou, Y. Zhou, M. Zhou, X. Su, P. Cheng, The enhanced near-infrared fluorescence of Nd^{3+} doped tellurite glass. J. Non-Cryst. Solids **470**, 122–131 (2017)

45. K. Nasser, V. Aseev, S. Ivanov, A. Ignatiev, N. Nikonorov, Optical, spectroscopic properties and Judd–Ofelt analysis of Nd^{3+} doped photo-thermo-refractive glass. J. Lumin. **213**, 255–262 (2019)

46. J. Krogh-Moe, The structure of vitreous and liquid boron oxide. J. Non-Cryst. Solids **1**, 269–284 (1969)

47. E.I. Kamitsos, A.P. Patsis, M.A. Karakassides, G.D. Chryssikos, Infrared reflectance spectra of lithium borate glasses. J. Non-Cryst. Solids **126**, 52–67 (1990)

48. F.H. ElBatal, M.A. Marzouk, Y.M. Hamdy, H.A. ElBatal, Optical and FT infrared absorption spectra of 3d transition metal ions doped in NaF–CaF_2–B_2O_3 glass and effects of gamma irradiation. J. Solid State Phys. **2014**, 1–8 (2014). https://doi.org/10.1155/2014/389543

49. J. Wong, C.A. Angell, *Glass Structure by Spectroscopy* (Marcel Dekker, New York, 1976)

50. E.I. Kamitsos, A.P. Patsis, G.D. Chryssikos, Infrared reflectance investigation of alkali diborate glasses. J. Non-Cryst. Solids **152**, 246–252 (1993)

51. K.R.S. Pasha, V.C.V. Gowda, N. Hanumantharaju, C.N. Reddy, Effect of Li_2SO_4 on the structure and properties of lithium lead borate glasses containing neodymium ions. Int. J. Appl. Eng. Res. **14**(6), 1426–1430 (2019)

52. Y.K. Dasan, B.H. Guan, M.H. Zahari, L.K. Chuan, Influence of La^{3+} substitution on structure, morphology and magnetic properties of nanocrystalline Ni–Zn ferrite. PLoS ONE **12**(1), e0170075 (2017). https://doi.org/10.1371/journal.pone.0170075

53. D.S. Pytalev, D. Caurant, O. Majérus, H. Trégouët, T. Charpentier, B.N. Mavrin, Structure and crystallization behavior of La_2O_3–$3B_2O_3$ metaborate glasses doped with Nd^{3+} or Eu^{3+} ions. J. Alloy. Compd. **641**, 43–55 (2015)

54. F.H. ElBatal, M.A. Marzouk, H.A. ElBatal, F.M. EzzElDin, Impact effect of gamma irradiation on the optical, FTIR, ESR spectral properties and thermal behavior of some mixed (PbO + Bi_2O_3) borate glasses searching for shielding effects. J. Mol. Struct. **1267**, 133602 (2022)

55. A.A. Abul-Magd, A.S. Abu-Khadra, A.M. Abdel-Ghany, Influence of La_2O_3 on the structural, mechanical and optical features of cobalt doped heavy metal borate glasses. Ceram. Int. **47**, 19886–19894 (2021)

56. C. Gautam, A.K. Yadav, A.K. Singh, A review on infrared spectroscopy of borate glasses with effects of different additives. Int. Sch. Res. Netw. (ISRN Ceram.) **2012**, 428497 (2012)

57. S. Arunkumar, K. Venkata Krishnaiah, K. Marimuthu, Structural and luminescence behavior of lead fluoroborate glasses containing Eu3þ ions. Physica B **416**, 88–100 (2013)